Responsive Telechelic Block Copolymers for Enhancing the Elasticity of Nanoemulsions

Daniel P. Keane, Matthew D. Mellor, and Ryan Poling-Skutvik*

Cite This: https://doi.org/10.1021/acsanm.1c03666

Read Online

ACCESS | Metrics & More | Article Recommendations | Supporting Information

ABSTRACT: The rheology of emulsions dictates their performance in many scientific and industrial applications. Here, we demonstrate that high-molecular-weight telechelic triblock copolymers composed of polystyrene end blocks with a poly(ethylene oxide) midblock effectively modify the rheology of a suspension of cyclohexane nanodroplets. Because of their telechelic structure, these polymers bridge between droplets to generate elastic networks with shear moduli on the order of 1000 Pa. The network elasticity increases with polymer concentration and molecular weight as the polymers more effectively form bridges. Furthermore, we tune the nanoscale interactions that control the polymer partitioning by decreasing the temperature below the cloud point of the system. At low temperatures, the polystyrene end blocks no longer preferentially partition into the cyclohexane droplets, and the emulsions begin to exhibit terminal viscous relaxations. These results identify key properties of telechelic block copolymers that can be exploited to significantly enhance nanoemulsion elasticity to improve the processability and transport of complex fluids in applications ranging from 3D printing to functional hydrogels.

KEYWORDS: nanoemulsions, telechelic polymers, rheology, elasticity, upper-critical solution temperature
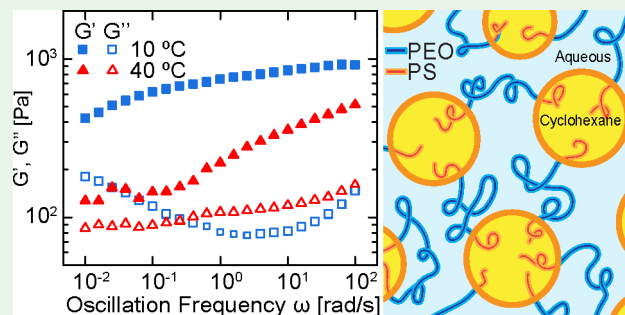
1. INTRODUCTION

Emulsions are a class of complex fluids widely encountered in scientific and industrial applications ranging from sweep fluids in the petroleum industry[1] to cosmetics and personal care products.[2] When stabilized by small molecule surfactants or other surface-active species,[3−5] emulsion droplets interact through nearly hard-sphere interactions, resulting in suspensions whose mechanical properties are largely dictated by a single physical parameter, the droplet volume fraction ϕ.[6,7] This simplicity makes emulsions ideal systems for investigating physical phenomena such as glassy dynamics,[8] cooperative rearrangements,[9,10] and the jamming transition,[11,12] but it also limits their tunability.

Applications such as 3D printing,[13] injection molding,[14] and drug delivery[15] often require that emulsions be pumped, sprayed, and extruded. During these processes, emulsions are subjected to complex deformations that can significantly distort their structure[16] and deleteriously affect their performance. Introducing specific rheological properties such as a yield stress[17,18] or linear elasticity[7] can ensure that the emulsion system maintains its functionality during and after processing. It remains challenging, however, to introduce these rheological properties into neat emulsions because of their simple physical interactions. Instead, desired rheological properties are commonly introduced by incorporating additives such as linear polymer chains.

Linear polymeric additives tune emulsion properties by modifying the rheology of the continuous phase or by inducing structural changes. When dispersed in the continuous phase, linear polymers interpenetrate and entangle to increase the suspension viscoelasticity according to established scaling laws.[19] Additionally, polymer chains may induce structural changes in the suspension, such as the formation of depletion gels.[20] Depletion gels form as colloids aggregate to minimize the polymer excluded volume,[21−23] resulting in a percolated network of particles that increases the suspension viscosity and generates a yield stress. Because of their entropic bonds, however, depletion gels tend to be relatively weak and brittle.[24−27] By contrast, particle networks formed by polymeric bonds can exhibit significant extensibility, as the polymers stretch and rearrange to accommodate the applied strain.[28,29]

These polymeric bonds are often formed by associative polymers,[30,31] which possess attractive groups that bind to dispersed particles.[32−36] Telechelic polymers are a unique class

of associating polymers possessing attractive groups only at their ends, making them especially useful because their interaction strength can be easily tuned by varying their end-group chemistry.[37] This chemistry can be exploited to drive self-assembly in solution[38−40] or to induce structural changes in emulsions.[41−44] Despite the potential of telechelic polymer additives to serve as facile rheological modifiers, it remains challenging to predict and control the properties of the resulting network.

Here, we investigate the effect of high-molecular-weight telechelic block copolymers on the elasticity of a suspension of emulsion nanodroplets. The emulsion is composed of cyclohexane stabilized by a mixture of nonionic surfactants to which the triblock copolymer poly(styrene)-b-poly(ethylene oxide)-b-poly(styrene) (SEOS) is added. This system exploits the thermodynamic partitioning of the polystyrene end blocks into the cyclohexane droplets so that the polymer chains form bridges that contribute to the formation of an elastic network. We vary both the polymer concentration and molecular weights and quantify the emulsion moduli using oscillatory rheology. The moduli increase with increasing polymer concentration and molecular weight as the chains more effectively bridge between nanodroplets. Furthermore, we exploit the upper-critical solution temperature (UCST) behavior of the polystyrene/cyclohexane system to evaluate the effects of the interaction parameter χ. At temperatures below the cloud-point of the system, the end blocks no longer preferentially partition into the cyclohexane nanodroplets and the emulsions begin to exhibit terminal relaxations. These findings demonstrate how polymer properties can be exploited to tune emulsion elasticity.

2. MATERIALS AND METHODS

2.1. Materials. Cyclohexane (≥99% purity), Tween 20, and Span 20 were purchased from Sigma-Aldrich. Three different molecular weights of poly(styrene)-b-poly(ethylene oxide)-b-poly(styrene) (SEOS) were purchased from PolymerSource and used without further modification. Poly(ethylene oxide) (PEO) was purchased from Scientific Polymer. The properties and nomenclature of these polymers are listed in Table 1. Additionally, polystyrene (PS) with M_n of 32.4 kDa (Đ = 1.03) and 12.0 kDa (Đ = 1.01) were purchased from Scientific Polymer.

Table 1. Nomenclature, Number Average Molecular Weight M_n, and Dispersity Đ of Polymers Used in This Study

polymer	M_n [kDa] (PS-b-PEO-b-PS)	Đ
SEOS-180/32	32-b-180-b-32	1.10
SEOS-180/10	10-b-180-b-10	1.10
SEOS-27/11.5	11.5-b-27-b-11.5	1.09
PEO	0-b-223.2-b-0	1.04

2.2. Emulsion Preparation. Cyclohexane-in-water emulsions with a volume fraction $\phi = 0.5$ were produced through sonication in the following manner (Figure 1). First, Tween 20 with a hydrophilic−lipophilic balance (HLB) of 16.7 was mixed with Span 20 (HLB = 8.6) at a weight ratio of 4:1 to form a nonionic surfactant mixture with HLB = 15.0. This surfactant mixture was then diluted with deionized (DI) water to the desired concentration of 17.0 g/L. Nanoemulsions were prepared in batches of 6 mL by adding 3 mL of cyclohexane dropwise at a rate of 0.3 mL/min to the diluted surfactant solution under sonication at an amplitude of 30% on a 40 kHz Branson SLPe digital sonifier fitted with a 1/8 in. tapered microtip. Sonication was stopped 2 min after the full addition of cyclohexane to ensure effective emulsification. The desired quantity of

polymer was then added to the nanoemulsion, the vial sealed to prevent evaporation, and the emulsion stirred at 50 °C until the polymer was fully dissolved. Emulsions were prepared at nominal SEOS concentrations of 1, 3, and 5 wt %, which correspond to 9.0, 28, and 47 g/L, respectively. The prepared emulsions were stable for up to a month, but showed signs of creaming on longer time scales.

2.3. Drop Shape Analysis. A Krüss DSA-100 instrument was used to measure the interfacial tension between cyclohexane and the water−surfactant mixture using the pendant drop method.[45] A 27 gauge needle dispensed a 2 μL drop of surfactant solution into cyclohexane. The interfacial tension between cyclohexane and the surfactant solution was determined to be 7.9 ± 0.2 mN/m by fitting the contour of the droplet to a system of differential equations outlined by the Young−LaPlace method.

2.4. Dynamic Light Scattering. Dynamic light scattering (DLS) was conducted on a BI-200SM goniometer fitted with a Brookhaven Instruments Mini L40 compact diode laser with a wavelength of $\lambda_0 = 640$ nm. Samples were diluted by ∼200× with DI water prior to taking five measurements at each of five angles ranging from $\theta = 60−120°$. The resulting intensity autocorrelation functions g_2 were fit to either a stretched exponential given by

$$g_2(\tau) = A + B\exp(-2(\Gamma\tau)^\beta) \tag{1}$$

to capture a single polydisperse population or to the sum of two stretched exponentials given by

$$g_2(\tau) = A + B[f\exp(-(\Gamma_1\tau)^{\beta_1}) + (1-f)\exp(-(\Gamma_2\tau)^{\beta_2})]^2 \tag{2}$$

to capture two populations. In these expressions, τ is the delay time, Γ_i is the relaxation rate, and β_i is a stretching exponent that quantifies the polydispersity of the particle sizes. A, B, and f are constants that describe the long and short time plateaus and the fraction of the signal intensity contributed by the first decay, respectively. The normalized value $\bar{\Gamma} = \Gamma\beta/\Gamma^*(1/\beta)$, where Γ^* is the Gamma function, allows for comparisons of Γ across different values of β.[46] The nanodroplet diffusivity is calculated by $D_T = \bar{\Gamma}q^2$, where q is the wavevector defined by $q \equiv 4\pi n \sin(\theta/2)/\lambda_0$, and $n = 1.333$ is the refractive index of water. The hydrodynamic diameter d_H of the nanodroplets is determined by the Stokes−Einstein equation $d_H = k_B T/3\pi\eta D_T$, where k_B is the Boltzmann constant, T is the temperature, and η is the solvent viscosity.

2.5. Rheology. Rheology measurements were performed on a stress-controlled TA Instruments Discovery hybrid rheometer (HR20) with a Peltier temperature controller. Depending upon sample viscosity and volume restrictions, samples were characterized using cone-and-plate geometries with diameters of either 20 or 60 mm, or a concentric cylinder geometry with a bob diameter of 28 mm and a cup diameter of 30 mm. The polymer-free emulsion was characterized in the concentric cylinder, and the 60 mm cone-and-plate was used to characterize all emulsions containing PEO as well as those containing either 9.0 or 28 g/L of any SEOS species. Emulsions containing 47 g/L SEOS were characterized with the 20 mm cone-and-plate. All samples were enclosed by a solvent trap to minimize sample evaporation and allowed to equilibrate for 15 min under small-amplitude oscillation. For either cone-and-plate geometry, the solvent trap was sealed with mineral oil and its interior was saturated with cyclohexane as additional precautions against evaporation. With these precautions, evaporation and creaming effects are negligible over experimental time scales of at least 2.5 h (see the Supporting Information). All oscillatory measurements were performed within the linear viscoelastic (LVE) region at a strain $\gamma = 0.3\%$. Data acquired below the machine torque limit of 0.1 nN m or above the raw phase limit of 170° were removed to account for artifacts arising from instrumental inertia. At least three trials were conducted for each sample.

3. RESULTS AND DISCUSSION

3.1. Establishing an Elastic Network. Because of its telechelic nature, the SEOS polymer is expected to assemble at
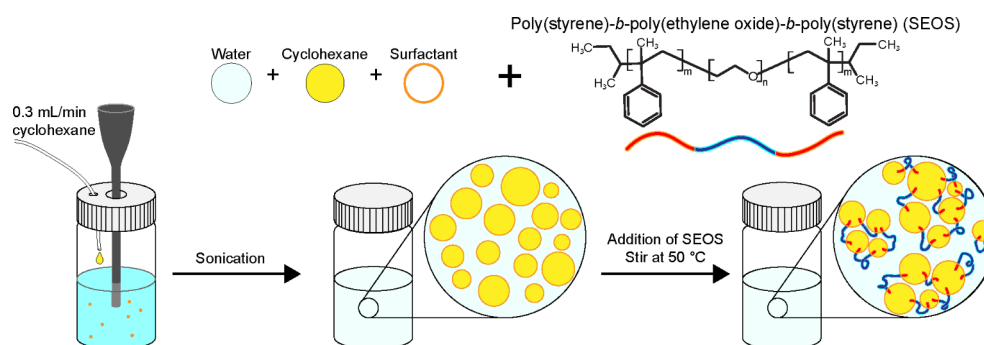
Figure 1. Schematic illustrating the emulsion preparation process, in which cyclohexane is added dropwise to an aqueous surfactant solution under sonication and then mixed with the appropriate amounts of polymer.

the cyclohexane-water interface so that the hydrophobic polystyrene (PS) end blocks are located within the cyclohexane nanodroplets and the hydrophilic poly(ethylene oxide) (PEO) midblock is located in the continuous aqueous phase. To satisfy this condition, SEOS is expected to take on one of two conformations—bridging between nanodroplets such that each PS end block is located in a different droplet or looping on a droplet such that both PS end blocks are in the same droplet (Figure 2a). Additional conformations, such as dangling chains,[47] are possible but energetically unfavorable and therefore expected to be negligible. Although nonionic surfactants are used here, we expect the SEOS polymer to adopt similar configurations in the presence of ionic surfactants because the polymers are uncharged and the partitioning of the chains is controlled solely by thermodynamic polymer–solvent interactions. The bridging fraction $\sigma = n_{\text{bridging}}/n_{\text{total}}$ describes the fraction of total chains that bridge between droplets and has been found to depend on the nanodroplet size, dispersed phase volume fraction, and the molecular weight of each block.[48−51] We note that only bridging chains will generate a network, whereas looping chains will act as defects that do not contribute to the enhanced elasticity of the emulsions.

To confirm that SEOS successfully bridges between nanodroplets, we use DLS to analyze the dynamic relaxations of emulsions diluted by ∼200× with DI water. For diluted neat emulsions, the DLS autocorrelation function g_2 follows a single stretched exponential decay (Figure 2b), corresponding to an average particle diameter of $d_H = 390 \pm 30$ nm with a stretching exponent $\beta = 0.76 \pm 0.06$. This stretching exponent indicates that the emulsion is formed by a moderately polydisperse population of cyclohexane droplets. We confirm that the parameters extracted from the stretched exponential fits are consistent with values extracted from two-parameter cumulant fits.[52] For emulsions containing dissolved SEOS polymer, however, g_2 of the diluted sample exhibits a second decay. Although there are many methods to extract particle dynamics from g_2, including numerical inversion methods such as CONTIN, we choose to fit the two-step decay with a sum of stretched exponentials (eq 2). This fitting procedure is commonly used in literature to explicitly capture two distinct populations.[53]

For the diluted SEOS emulsion, the first decay corresponds to an average particle size of $d_H = 400 \pm 20$ nm with a stretching exponent $\beta = 0.84 \pm 0.07$. Within experimental uncertainty, this first population is indistinguishable from that measured in the neat emulsion (inset to Figure 2b), indicating that the addition of SEOS does not significantly affect the size of individual droplets. The second decay occurs at a longer
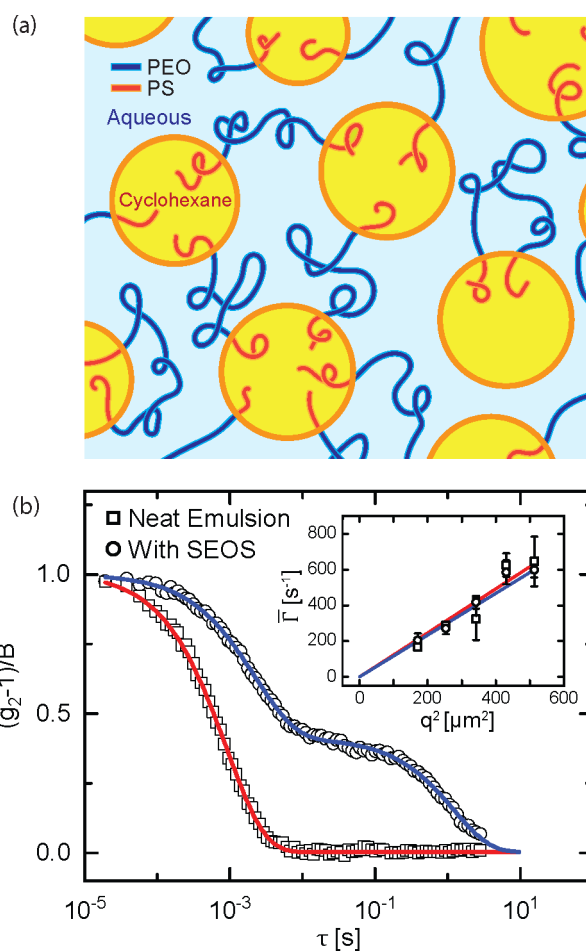

Figure 2. (a) Schematic illustrating possible looping and bridging conformations of SEOS. (b) Normalized autocorrelation function $(g_2 - 1)/B$ as a function of time τ. Curves are fits to eqs 1 and 2. All DLS measurements were taken at $T = 21$ °C. The SEOS-containing sample was diluted by a factor of ∼200× from an emulsion containing 28 g/L SEOS-180/32. Inset: Normalized relaxation rate $\bar{\Gamma}$ as a function of q^2. Error bars represent one standard deviation.

times and thus corresponds to the presence of larger structures, which is consistent with visual observations of macroscopic particulates that fail to fully disperse when the emulsion is diluted (see the Supporting Information). We attribute these structures to polymer-linked clusters of nanodroplets. With $\bar{\Gamma} = 0.33 \pm 0.09$ s^{-1} and $\beta = 0.87 \pm 0.09$, this second decay would correspond to a cluster size of $d_H \approx 370 \pm 120$ μm, but this size is beyond the limit of Brownian motion. When particles

are this large, viscous forces dominate thermal fluctuations to invalidate the assumptions of the Stokes−Einstein expression.[54] Instead, we expect the decorrelation to occur as the cyclohexane clusters cream to the top of the sample due to the liquid density difference. Indeed, the second decay disappears over time but reappears when the sample is inverted to redisperse the droplets and clusters. For these reasons, we cannot accurately estimate the cluster size from DLS. Nevertheless, the appearance of the second decay demonstrates that the SEOS polymer successfully links the nanodroplets into networks.

After confirming that the SEOS polymers effectively bridge between emulsion droplets, we explore the effect of this bridging on the rheological properties of the emulsions. We first identify the linear viscoelastic region using an oscillatory amplitude sweep at constant frequency (Figure 3). At low
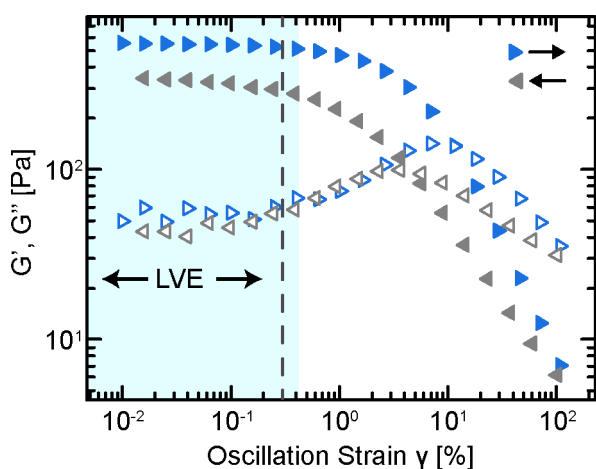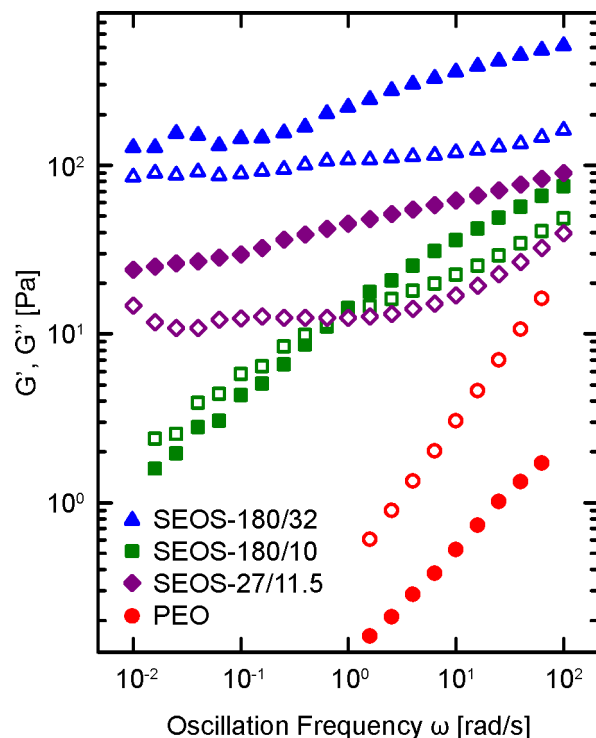

Figure 3. Storage modulus G' (closed symbols) and loss modulus G'' (open symbols) at $\omega = 10$ rad/s and $T = 40$ °C as a function of oscillation strain γ for an emulsion containing 28 g/L SEOS-180/32. The shaded area indicates the linear viscoelastic (LVE) region, and the vertical dashed line indicates the strain $\gamma = 0.3\%$ used for future oscillatory measurements. Blue and gray points represent data acquired during up and down sweeps with increasing and decreasing γ, respectively.

strain amplitude $\gamma < 0.4\%$, the linked emulsion system responds as an elastic solid with the storage modulus G' larger than the loss modulus G''. For $\gamma > 0.4\%$, however, the material enters the nonlinear regime. In this regime, the elastic modulus G' decreases rapidly and G'' initially increases to develop an overshoot at $\gamma \approx 10\%$, which are both typical characteristics of a yield-stress fluid.[55,56] Qualitatively similar behavior is observed for all SEOS emulsions. After the sample is yielded, we measure the recovery of network properties through a second amplitude sweep from high to low strains (Figure 3). As γ decreases, the material transitions from viscous flow back to elastic deformation. During this recovery, the peak in G'' is suppressed and shifted to lower strains, and the emulsion fails to fully recover its original elastic modulus. These characteristics indicate that the yielding process is irreversible. Physically, we expect this irreversible yielding to occur because the PS end blocks are pulled out of the cyclohexane droplets at high strains and then reimbed in a new cyclohexane droplet to form either a new bridge or loop. Thus, yielding acts to transition some bridges into loops, weakening the network and reducing the elasticity of the material. Because

of the irreversible nature of this process, quantifying the nonlinear properties of this system requires carefully designed rheological procedures and remains a significant challenge that will be addressed in future work. For the rest of this work, we will focus on characterizing the linear rheological properties of these linked emulsion networks.

3.2. Effects of Polymer Properties. Frequency sweeps of the linked nanoemulsions indicate that their rheology strongly depends on polymer properties (Figure 4). Emulsions

Figure 4. Storage modulus G' (closed symbols) and loss modulus G'' (open symbols) at $T = 40$ °C as a function of oscillation frequency ω for emulsions containing 28 g/L polymer.

prepared with the highest M_n SEOS-180/32 polymer are highly elastic with a large G' that decreases only slightly with decreasing ω. Furthermore, G' of the SEOS-180/32 sample exhibits a plateau at low ω, indicating that the sample is fully elastic without undergoing any observable terminal relaxations. By contrast, emulsions produced with the same concentration of the SEOS-180/10 polymer, which has lower M_n end blocks but a comparable midblock, have much lower moduli and exhibit clear terminal relaxations in which $G'' > G'$ at low ω. The SEOS-27/11.5 polymer has a lower M_n midblock but produces emulsions with intermediate moduli that slowly decrease with decreasing ω. Similar qualitative trends are observed for emulsions prepared at different polymer concentrations (see the Supporting Information). The observed changes to the relaxation spectra demonstrate that the end- and midblock M_n control the rheological properties of the linked nanoemulsions.

We confirm that these changes are caused by the bridging of the SEOS polymer by comparing their rheology to that of an emulsion prepared with neutral PEO chains of a similar molecular weight (Table 1). PEO chains are expected to dissolve entirely in the continuous aqueous phase of the emulsion because of their lack of hydrophobic end groups. The
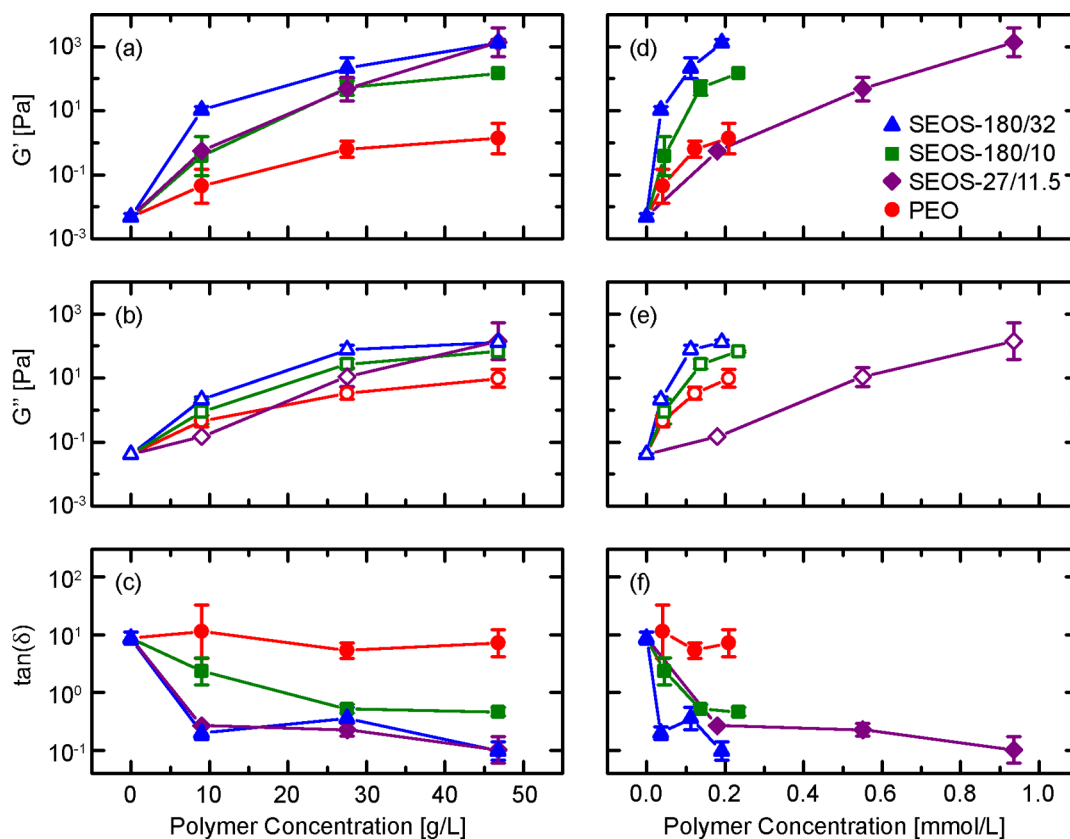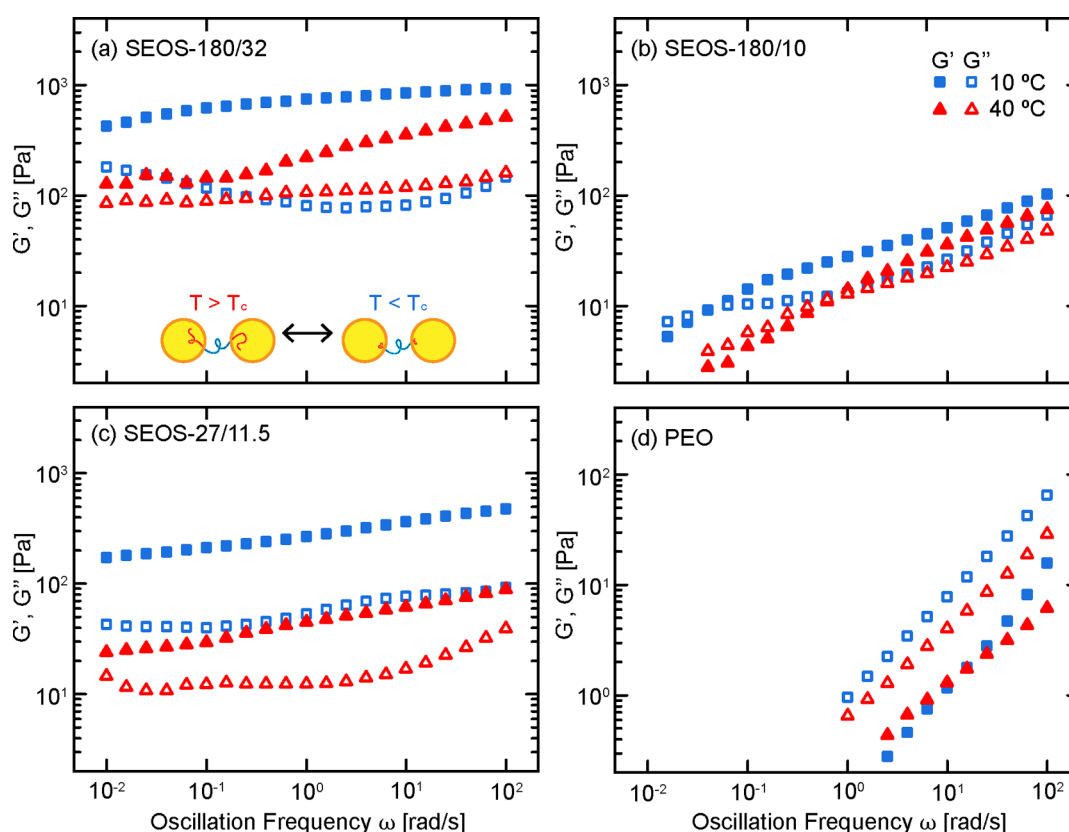
Figure 5. (a, d) Storage modulus G', (b, e) loss modulus G'', and (c, f) $\tan(\delta)$ at $T = 40\,°C$ and $\omega = 10$ rad/s for emulsions prepared with various polymers as a function of (a–c) mass concentration and (d–f) molar concentration. Error bars represent one log-normal standard deviation.

resulting emulsions are mostly viscous (i.e., $G'' > G'$) with rheology nearly indistinguishable from that of a neat PEO solution at a comparable concentration (see the Supporting Information). These results indicate that although non-associating chains do increase the viscosity of the cyclohexane emulsions, they cannot generate the elasticity observed for telechelic polymers.

The rheological properties of the linked emulsion networks also depend on the concentration of polymer additives. For all polymers, both G' and G'' increase with increasing polymer concentration, but the rate of change depends on the M_n of both blocks of the copolymer (Figure 5a, b). The higher M_n SEOS-180/32 increases the emulsion moduli more rapidly than the lower M_n species SEOS-180/10 and SEOS-27/11.5. Additionally, the network elasticity is similar for emulsions containing SEOS-180/32 and SEOS-27/11.5 as quantified through $\tan(\delta) = G''/G'$, but the network formed by SEOS-180/10 is much less elastic at comparable mass concentrations (Figure 5c). In all cases, the networks formed by SEOS polymers are more elastic and have higher moduli than emulsions prepared with the nonassociating PEO chains. From these trends, both SEOS-180/32 and SEOS-27/11.5 appear equally effective in enhancing the emulsion elasticity. When the rheological properties are plotted against molar concentrations (Figure 5d–f), however, a clear trend develops. The storage modulus of the network increases most rapidly as a function of molar concentration for SEOS-180/32, followed by SEOS-180/10, PEO, and finally, SEOS-27/11.5. Because molar concentration quantifies the number density of chains, this trend indicates that the SEOS-180/32 chains are more effective at generating a strong, elastic network on a per chain basis.

From these observations, we can begin to construct a theoretical understanding of how telechelic triblock copolymers enhance the rheological properties of linked emulsions. For polymeric materials, the modulus G of an elastic network is typically described according to the affine network model, which gives $G \approx \nu k_B T$, where ν is the number density of chains participating in the network.[19] In this system, only bridging chains will contribute to the network[57] so that $G \approx \sigma \nu_t k_B T$, where ν_t represents the number density of total chains in the system. Therefore, we expect the bridging fraction σ to play a dominant role in controlling the emulsion moduli. Previous studies[58,59] find that σ is predominantly controlled by the ratio $\alpha = D_{ID}/R_g$, where $D_{ID} = d_H\big[(\phi_{max}/\phi)^{1/3} - 1\big] \approx 34$ nm is the surface-to-surface spacing between droplets[60] and $\phi_{max} = 0.64$ is the volume fraction at random close packing. The radius of gyration R_g of the polymer chains is estimated to be 22 and 7.3 nm for free PEO chains[61] with $M_n = 180$ kDa and 27 kDa, respectively. With these estimates, we calculate that $\alpha = 1.5$ and 4.6 for SEOS chains with midblock sizes of 180 and 27 kDa, respectively. Although ϕ is well-controlled in our emulsions by the amount of cyclohexane added during emulsification, the polydispersity of droplets will lead to a distribution in D_{ID} and therefore a distribution in α. At low α, the distance between droplets is small relative to the size of the polymer, meaning that the polymer has a relatively high likelihood of forming a bridge. As α increases, σ decreases because bridge formation becomes energetically unfavorable as it requires the polymer to entropically stretch.

On the basis of the Monte Carlo simulations of Testard et al.,[59] these estimated α values correspond to $\sigma \approx 0.2$ and 0.02 for SEOS-180/32 and SEOS-27/11.5, respectively. This order-

Figure 6. Storage modulus G' (closed symbols) and loss modulus G'' (open symbols) as a function of frequency ω for emulsions containing 28 g/ L: (a) SEOS-180/32, (b) SEOS-180/10, (c) SEOS-27/11.5, and (d) PEO at both $T = 10$ °C (blue) and $T = 40$ °C (red). Inset: Schematic demonstrating the conformational changes of the PS end blocks across T_θ.

of-magnitude higher bridging fraction qualitatively explains the higher moduli for emulsions prepared with SEOS-180/32 relative to those prepared with SEOS-27/11.5 on a per chain basis (Figure 5d). The lower M_n of SEOS-27/11.5, however, largely offsets this difference in σ by increasing the chain number density to give comparable moduli when polymer concentration is considered on a mass concentration basis (Figure 5a). Using these bridging fractions, we estimate the elastic moduli of emulsions prepared with 28 g/L of SEOS with 180 and 27 kDa midblocks to be on the order of 50 and 20 Pa, respectively, in good agreement with experimental findings.

This difference in bridging fraction, however, cannot explain the difference observed between SEOS-180/32 and SEOS-180/10, which only differ in the M_n of the PS end blocks. In this case, we expect a secondary contribution to emulsion properties to arise from the strength of thermodynamic interactions localizing the PS end blocks within the cyclohexane droplets. Polymer phase behavior is well described by the Flory[62]−Huggins[63] interaction parameter χ, which can be straightforwardly expanded to describe the partitioning of polymers in a ternary system according to the difference in interaction parameters $\Delta\chi$.[64,65] In this system, $\Delta\chi$ corresponds to the difference between the PS/water and PS/cyclohexane interaction parameters. Similarly, the self-assembly of block copolymers[66] is controlled by the product χN, where N is the degree of polymerization. Merging these descriptions, we expect that the partitioning of the PS end blocks is controlled by $\Delta\chi N$ such that the SEOS polymers with larger M_n end blocks partition more strongly. This partitioning may affect the

emulsion properties in two ways. First, the larger M_n end blocks will result in stronger effective cross-links that enhance the network modulus.[67] Second, the stronger partitioning should result in a higher fraction of bridging chains by slowing the kinetics of bridge-to-loop transitions.[68,69]

Our finding that telechelic polymers with higher M_n end blocks lead to more elastic emulsions is consistent with previous studies using telechelic polymers with oligomeric C18-end blocks.[70,71] These studies find that polymers with oligomeric end blocks significantly thicken a microemulsion suspension but fail to induce the same degree of elasticity observed in this study. In contrast to the low-ω plateau observed in our emulsions (Figure 4), the microemulsions thickened by C18-linkers display viscous behavior with terminal relaxations. We expect that this difference is caused by different energy barriers controlling the end block partitioning. In our system, the high M_n end blocks leads to a large $\Delta\chi N$ and a significant energy barrier that prevents the end blocks from partitioning into the continuous phase. In the case of oligomeric end blocks, however, $\Delta\chi N$ is much smaller so that the end blocks can partition into the continuous phase to break and reform the elastic network. This difference in energy barriers explains how emulsions prepared with oligomeric linkers are thickened but viscous, whereas our emulsions prepared with high M_n linkers remain elastic even at low ω. Moreover, this physical picture is consistent with the different relaxations observed for the SEOS-180/32 and SEOS-180/10 samples.

3.3. Thermally Driven Nanoscale Changes. In addition to controlling $\Delta\chi N$ by changing the length of the PS end block,

we can test the effect of the thermodynamically controlled partitioning by varying the temperature across the M_n-dependent upper-critical solution temperature T_θ for polystyrene in cyclohexane.[72] For $T > T_\theta$, cyclohexane acts as a good solvent (i.e., $\chi < 0.5$) and swells the PS chains, but for $T < T_\theta$ cyclohexane acts as a poor solvent (i.e., $\chi > 0.5$), resulting in the PS chains collapsing into globules.[72,73] We confirm this conformational change by observing the turbidity of a solution of free PS chains with comparable M_n to the SEOS end blocks. For $M_n = 32.4$ kDa, the solution becomes turbid for $T < 11$ °C, in agreement with literature values (see the Supporting Information). For $M_n = 12$ kDa, however, the cyclohexane freezes before the cloud-point is reached. Therefore, we assess the effects of $\Delta\chi$ by comparing the rheological curves for $T > T_\theta$ to those measured at $T < T_\theta$.

For emulsions prepared with PEO or the SEOS polymers with low-M_n PS end blocks, the rheological curves are shifted to lower frequencies at low T, but the shapes of the relaxations remain essentially unchanged (Figure 6). The shift to lower ω indicates that the relaxations in the emulsions are slower, consistent with an increase in the viscosity of the aqueous continuous phase; the similar shape of the frequency sweeps, however, indicate that the change in temperature does not fundamentally affect the nature of the relaxations in the system. By contrast, the frequency sweeps for the emulsion containing the SEOS-180/32 polymer exhibit markedly different behaviors as a function of temperature (Figure 6a). At high T, the SEOS-180/32 emulsion exhibits a clear elastic plateau at low frequency, as previously discussed. Below T_θ, however, the low-ω plateau disappears, and the emulsion shows signs of undergoing terminal relaxations. This change in the relaxation spectrum of the emulsion indicates that the droplets now viscously rearrange on long time scales rather than participating in an elastic network. Furthermore, we observe qualitatively similar changes in the relaxations for all emulsions prepared at different concentrations of the SEOS-180/32 polymer (Figure 7). In all cases, the sweeps at high temperatures show clear elastic plateaus at low ω that disappear when $T < T_\theta$.

The observed rheological changes indicate that $\Delta\chi$ has a profound effect on the elasticity of emulsions containing telechelic block copolymers. As discussed previously, we find that the difference in interaction parameters $\Delta\chi N$ controls the degree of partitioning of the telechelic end blocks into the cyclohexane droplets. At low temperatures, the PS/cyclohexane interaction parameter becomes unfavorable and approaches that of PS/water so that $\Delta\chi N$ approaches zero. In this fashion, decreasing $T < T_\theta$ reduces the enthalpic interactions controlling the partitioning of the PS end blocks in the cyclohexane droplets, and the telechelic chains no longer act as cross-links. Without strong enthalpic interactions promoting the partitioning of end blocks into the dispersed droplets, the telechelic polymers fail to produce a fully elastic network.

4. CONCLUSIONS

In this work, we demonstrate that telechelic block copolymers efficiently bridge between emulsion droplets to generate an elastic network. Polymers with higher-molecular-weight mid- and end blocks generate stronger networks by increasing the fraction of bridging chains and strengthening the partitioning of the end blocks, respectively. Furthermore, we directly test the effect of the interaction parameter χ by varying the
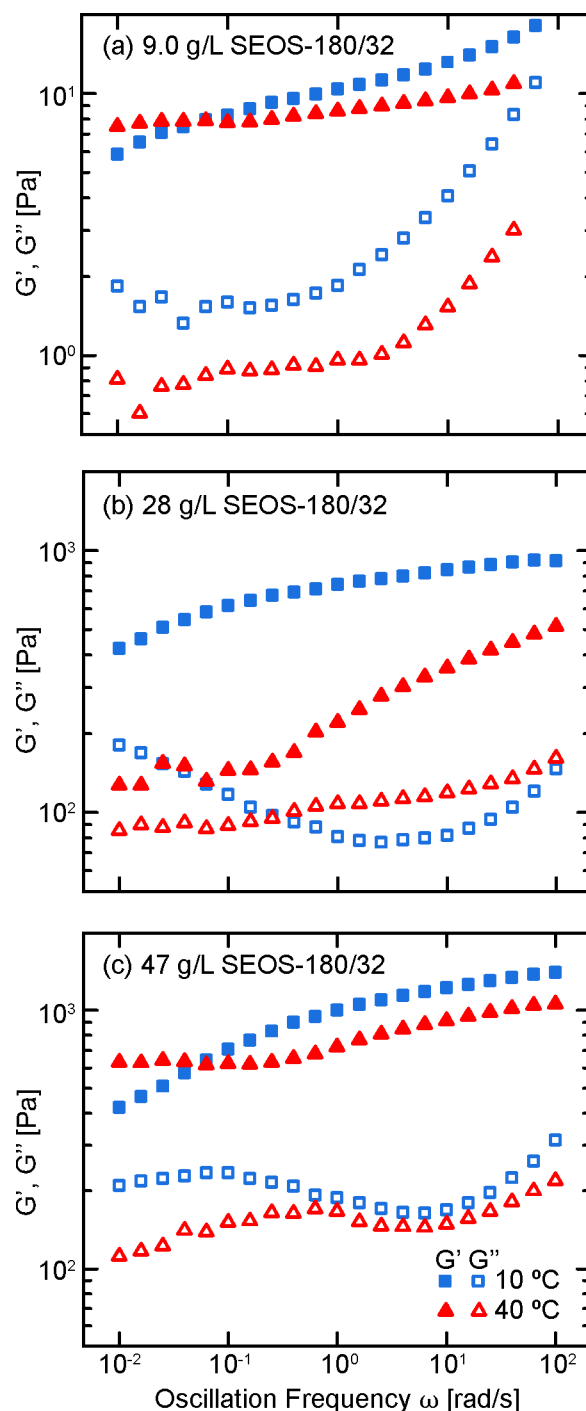
Figure 7. Storage modulus G' (closed symbols) and loss modulus G'' (open symbols) as a function of oscillation frequency ω for emulsions containing SEOS-180/32 at concentrations of (a) 9.0 g/L, (b) 28 g/L, and (c) 47 g/L at both $T = 10$ °C (blue) and $T = 40$ °C (red).

temperature across the polystyrene/cyclohexane cloud point. For low-M_n end blocks that do not undergo a significant conformational change at low temperatures, the relaxations in the emulsion are slowed but not fundamentally altered. For high-M_n end blocks, however, the low-frequency elastic plateau disappears at low temperatures because of weaker partitioning of the end blocks into the cyclohexane droplets.

These findings serve as guiding principles to aid the design of complex fluids for applications such as 3D printing inks,[13,74,75] injectable therapeutics,[76,77] and functional hydro-

gels.[78,79] These applications require materials that flow under applied stress but possess finite elasticity at rest, the combination of which allows them to be easily processed and retain their shape after being delivered to regions of interest. Although emulsion-based systems promise enhanced functionality because of their distinct nanoscale structure, they often suffer from low elasticities and poor mechanical properties. This work demonstrates how telechelic block copolymers can serve as efficient rheological modifiers to tune and control the suspension elasticity through straightforward parameters including concentration, molecular weight, and temperature.

■ ASSOCIATED CONTENT

Ⓢ Supporting Information

The Supporting Information is available free of charge at https://pubs.acs.org/doi/10.1021/acsanm.1c03666.

> Oscillatory time sweep demonstrating the temporal stability of the emulsions, an image of clusters of nanodroplets, frequency sweeps of emulsions containing 47 g/L of added polymer, frequency sweeps of a PEO-containing emulsion and a PEO solution, and a visual depiction of the cloud point of 32 kDa polystyrene (PDF)

■ AUTHOR INFORMATION

Corresponding Author

Ryan Poling-Skutvik − *Department of Chemical Engineering, University of Rhode Island, Kingston, Rhode Island 02881, United States;* ⊙ orcid.org/0000-0002-1614-1647; Email: ryanps@uri.edu

Authors

Daniel P. Keane − *Department of Chemical Engineering, University of Rhode Island, Kingston, Rhode Island 02881, United States*

Matthew D. Mellor − *Department of Chemical Engineering, University of Rhode Island, Kingston, Rhode Island 02881, United States*

Complete contact information is available at:
https://pubs.acs.org/10.1021/acsanm.1c03666

Notes

The authors declare no competing financial interest.

■ ACKNOWLEDGMENTS

■ REFERENCES

(1) Schramm, L. L. In *Emulsions*; Schramm, L. L., Ed.; Advances in Chemistry; American Chemical Society: Washington, DC, 1992; Vol. 231; pp 1−49.

(2) Brummer, R.; Godersky, S. Rheological studies to objectify sensations occurring when cosmetic emulsions are applied to the skin. *Colloids Surfaces A Physicochem. Eng. Asp.* **1999**, *152*, 89−94.

(3) Binks, B. P. Particles as surfactants - Similarities and differences. *Curr. Opin. Colloid Interface Sci.* **2002**, *7*, 21−41.

(4) Horozov, T. S.; Binks, B. P. Particle-stabilized emulsions: A bilayer or a bridging monolayer? *Angew. Chemie - Int. Ed.* **2006**, *45*, 773−776.

(5) Maillard, D.; Kumar, S. K.; Rungta, A.; Benicewicz, B. C.; Prud'homme, R. E. Polymer-grafted-nanoparticle surfactants. *Nano Lett.* **2011**, *11*, 4569−73.

(6) Derkach, S. R. Rheology of emulsions. *Adv. Colloid Interface Sci.* **2009**, *151*, 1−23.

(7) Kim, H. S.; Mason, T. G. Advances and challenges in the rheology of concentrated emulsions and nanoemulsions. *Adv. Colloid Interface Sci.* **2017**, *247*, 397−412.

(8) Scheffold, F.; Cardinaux, F.; Mason, T. G. Linear and nonlinear rheology of dense emulsions across the glass and the jamming regimes. *J. Phys.: Condens. Matter* **2013**, *25*, 502101.

(9) Clara-Rahola, J.; Brzinski, T. A.; Semwogerere, D.; Feitosa, K.; Crocker, J. C.; Sato, J.; Breedveld, V.; Weeks, E. R. Affine and nonaffine motions in sheared polydisperse emulsions. *Phys. Rev. E* **2015**, *91*, 010301.

(10) Richards, J. A.; Martinez, V. A.; Arlt, J. Characterising shear-induced dynamics in flowing complex fluids using differential dynamic microscopy. *Soft Matter* **2021**, *17*, 8838−8849.

(11) Zhang, H. P.; Makse, H. A. Jamming transition in emulsions and granular materials. *Phys. Rev. E* **2005**, *72*, 011301.

(12) Desmond, K. W.; Young, P. J.; Chen, D.; Weeks, E. R. Experimental study of forces between quasi-two-dimensional emulsion droplets near jamming. *Soft Matter* **2013**, *9*, 3424−3436.

(13) Sommer, M. R.; Alison, L.; Minas, C.; Tervoort, E.; Rühs, P. A.; Studart, A. R. 3D printing of concentrated emulsions into multiphase biocompatible soft materials. *Soft Matter* **2017**, *13*, 1794−1803.

(14) Chen, Y.; Ballard, N.; Bon, S. A. Moldable high internal phase emulsion hydrogel objects from non-covalently crosslinked poly(N-isopropylacrylamide) nanogel dispersions. *Chem. Commun.* **2013**, *49*, 1524−1526.

(15) Porter, C. J. H.; Trevaskis, N. L.; Charman, W. N. Lipids and lipid-based formulations: optimizing the oral delivery of lipophilic drugs. *Nat. Rev. Drug Discovery* **2007**, *6*, 231−248.

(16) Windhab, E. J.; Dressler, M.; Feigl, K.; Fischer, P.; Megias-Alguacil, D. Emulsion processing - From single-drop deformation to design of complex processes and products. *Chem. Eng. Sci.* **2005**, *60*, 2101−2113.

(17) Balmforth, N. J.; Frigaard, I. A.; Ovarlez, G. Yielding to Stress: Recent Developments in Viscoplastic Fluid Mechanics. *Annu. Rev. Fluid Mech.* **2014**, *46*, 121−146.

(18) Nelson, A. Z.; Ewoldt, R. H. Design of yield-stress fluids: A rheology-to-structure inverse problem. *Soft Matter* **2017**, *13*, 7578−7594.

(19) Rubinstein, M., Colby, R. H. *Polymer Physics*; Oxford University Press: New York, 2003.

(20) Lu, P. J.; Zaccarelli, E.; Ciulla, F.; Schofield, A. B.; Sciortino, F.; Weitz, D. A. Gelation of particles with short-range attraction. *Nature* **2008**, *453*, 499−503.

(21) Asakura, S.; Oosawa, F. Interaction between particles suspended in solutions of macromolecules. *J. Polym. Sci.* **1958**, *33*, 183−192.

(22) Asakura, S.; Oosawa, F. On Interaction between Two Bodies Immersed in a Solution of Macromolecules. *J. Chem. Phys.* **1954**, *22*, 1255−1256.

(23) Binder, K.; Virnau, P.; Statt, A. Perspective: The Asakura Oosawa model: A colloid prototype for bulk and interfacial phase behavior. *J. Chem. Phys.* **2014**, *141*, 140901.

(24) Shah, S. A.; Chen, Y.-L.; Schweizer, K. S.; Zukoski, C. F. Viscoelasticity and rheology of depletion flocculated gels and fluids. *J. Chem. Phys.* **2003**, *119*, 8747−8761.

(25) Rueb, C. J.; Zukoski, C. F. Viscoelastic properties of colloidal gels. *J. Rheol.* **1997**, *41*, 197−218.

(26) van Doorn, J. M.; Verweij, J. E.; Sprakel, J.; van der Gucht, J. Strand Plasticity Governs Fatigue in Colloidal Gels. *Phys. Rev. Lett.* **2018**, *120*, 208005.

(27) Johnson, L. C.; Landrum, B. J.; Zia, R. N. Yield of reversible colloidal gels during flow start-up: Release from kinetic arrest. *Soft Matter* **2018**, *14*, 5048−5068.

(28) Bhatia, S. R.; Mourchid, A.; Joanicot, M. Block copolymer assembly to control fluid rheology. *Curr. Opin. Colloid Interface Sci.* **2001**, *6*, 471−478.

(29) Grosskopf, A. K.; Saouaf, O. A.; Lopez Hernandez, H.; Appel, E. A. Gelation and yielding behavior of polymer−nanoparticle hydrogels. *J. Polym. Sci.* **2021**, *59*, 2854−2866.

(30) Tam, K. C.; Jenkins, R. D.; Winnik, M. A.; Bassett, D. R. A structural model of hydrophobically modified urethane-ethoxylate (HEUR) associative polymers in shear flows. *Macromolecules* **1998**, *31*, 4149−4159.

(31) Tang, S.; Wang, M.; Olsen, B. D. Anomalous Self-Diffusion and Sticky Rouse Dynamics in Associative Protein Hydrogels. *J. Am. Chem. Soc.* **2015**, *137*, 3946−3957.

(32) Dickinson, E. Structure, stability and rheology of flocculated emulsions. *Curr. Opin. Colloid Interface Sci.* **1998**, *3*, 633−638.

(33) Gregory, J.; Barany, S. Adsorption and flocculation by polymers and polymer mixtures. *Adv. Colloid Interface Sci.* **2011**, *169*, 1−12.

(34) Chatterjee, T.; Nakatani, A. I.; Van Dyk, A. K. Shear-dependent interactions in hydrophobically modified ethylene oxide urethane (HEUR) based rheology modifier-latex suspensions: Part 1. molecular microstructure. *Macromolecules* **2014**, *47*, 1155−1174.

(35) Chatterjee, T.; Van Dyk, A. K.; Ginzburg, V. V.; Nakatani, A. I. Formulation-Controlled Positive and Negative First Normal Stress Differences in Waterborne Hydrophobically Modified Ethylene Oxide Urethane (HEUR)-Latex Suspensions. *ACS Macro Lett.* **2017**, *6*, 716−720.

(36) Van Dyk, A. K.; Chatterjee, T.; Ginzburg, V. V.; Nakatani, A. I. Shear-dependent interactions in hydrophobically modified ethylene oxide urethane (HEUR) based coatings: Mesoscale structure and viscosity. *Macromolecules* **2015**, *48*, 1866−1882.

(37) Tsarevsky, N. V.; Sumerlin, B. S.; Matyjaszewski, K. Step-growth "click" coupling of telechelic polymers prepared by atom transfer radical polymerization. *Macromolecules* **2005**, *38*, 3558−3561.

(38) Lo Verso, F.; Likos, C. N. End-functionalized polymers: Versatile building blocks for soft materials. *Polymer* **2008**, *49*, 1425−1434.

(39) Xia, Y.; Verduzco, R.; Grubbs, R. H.; Kornfield, J. A. Well-defined liquid crystal gels from telechelic polymers. *J. Am. Chem. Soc.* **2008**, *130*, 1735−1740.

(40) Wei, M.-H.; Li, B.; David, R. L. A.; Jones, S. C.; Sarohia, V.; Schmitigal, J. A.; Kornfield, J. A. Megasupramolecules for safer, cleaner fuel by end association of long telechelic polymers. *Science* **2015**, *350*, 72−75.

(41) Odenwald, M.; Eicke, H.-F.; Meier, W. Transient Networks by ABA Triblock Copolymers and Microemulsions: A Rheological Study. *Macromolecules* **1995**, *28*, 5069−5074.

(42) Blochowicz, T.; Gögelein, C.; Spehr, T.; Müller, M.; Stühn, B. Polymer-induced transient networks in water-in-oil microemulsions studied by small-angle x-ray and dynamic light scattering. *Phys. Rev. E* **2007**, *76*, 041505.

(43) Helgeson, M. E.; Moran, S. E.; An, H. Z.; Doyle, P. S. Mesoporous organohydrogels from thermogelling photocrosslinkable nanoemulsions. *Nat. Mater.* **2012**, *11*, 344−352.

(44) Helgeson, M. E.; Gao, Y.; Moran, S. E.; Lee, J.; Godfrin, M.; Tripathi, A.; Bose, A.; Doyle, P. S. Homogeneous percolation versus arrested phase separation in attractively-driven nanoemulsion colloidal gels. *Soft Matter* **2014**, *10*, 3122−3133.

(45) Berry, J. D.; Neeson, M. J.; Dagastine, R. R.; Chan, D. Y. C.; Tabor, R. F. Measurement of surface and interfacial tension using pendant drop tensiometry. *J. Colloid Interface Sci.* **2015**, *454*, 226−237.

(46) Patterson, G. D. Light Scattering from Bulk Polymers. *Annu. Rev. Mater. Sci.* **1983**, *13*, 219−245.

(47) Zinn, T.; Willner, L.; Knudsen, K. D.; Lund, R. Self-Assembly of Mixtures of Telechelic and Monofunctional Amphiphilic Polymers in Water: From Clusters to Flowerlike Micelles. *Macromolecules* **2017**, *50*, 7321−7332.

(48) Misra, S.; Mattice, W. L. Telechelic Polymers between Two Impenetrable Adsorbing Surfaces. *Macromolecules* **1994**, *27*, 2058−2065.

(49) Semenov, A. N.; Joanny, J.-F.; Khokhlov, A. R. Associating polymers: Equilibrium and linear viscoelasticity. *Macromolecules* **1995**, *28*, 1066−1075.

(50) Maccarrone, S.; Frielinghaus, H.; Allgaier, J.; Richter, D.; Lindner, P. SANS study of polymer-linked droplets. *Langmuir* **2007**, *23*, 9559−9562.

(51) Sarraguça, J. M. G.; Pais, A. A. C. C.; Linse, P. Influence of droplet properties on the formation of microemulsion-ABA-triblock copolymer networks. *Soft Matter* **2009**, *5*, 140−147.

(52) Frisken, B. J. Revisiting the method of cumulants for the analysis of dynamic light-scattering data. *Appl. Opt.* **2001**, *40*, 4087−4091.

(53) Hoffmann, I.; Simon, M.; Bleuel, M.; Falus, P.; Gradzielski, M. Structure, Dynamics, and Composition of Large Clusters in Polyelectrolyte-Surfactant Systems. *Macromolecules* **2019**, *52*, 2607−2615.

(54) Babick, F. *Characterization of Nanoparticles: Measurement Processes for Nanoparticles*; Elsevier, 2020; pp 137−172.

(55) Donley, G. J.; Singh, P. K.; Shetty, A.; Rogers, S. A. Elucidating the G″ overshoot in soft materials with a yield transition via a time-resolved experimental strain decomposition. *Proc. Natl. Acad. Sci. U. S. A.* **2020**, *117*, 21945−21952.

(56) Kamani, K.; Donley, G. J.; Rogers, S. A. Unification of the Rheological Physics of Yield Stress Fluids. *Phys. Rev. Lett.* **2021**, *126*, 218002.

(57) Pham, Q. T.; Russel, W. B.; Thibeault, J. C.; Lau, W. Micellar solutions of associative triblock copolymers: the relationship between structure and rheology. *Macromolecules* **1999**, *32*, 5139−5146.

(58) Milner, S. T.; Witten, T. A. Bridging Attraction by Telechelic Polymers. *Macromolecules* **1992**, *25*, 5495−5503.

(59) Testard, V.; Oberdisse, J.; Ligoure, C. Monte Carlo simulations of colloidal pair potential induced by telechelic polymers: Statistics of loops and bridges. *Macromolecules* **2008**, *41*, 7219−7226.

(60) Gam, S.; Meth, J. S.; Zane, S. G.; Chi, C.; Wood, B. A.; Winey, K. I.; Clarke, N.; Composto, R. J. Polymer diffusion in a polymer nanocomposite: effect of nanoparticle size and polydispersity. *Soft Matter* **2012**, *8*, 6512−6520.

(61) Bailey, F. E.; Kucera, J. L.; Imhof, L. G. Molecular weight relations of poly(ethylene oxide). *J. Polym. Sci.* **1958**, *32*, 517−518.

(62) Flory, P. J. Thermodynamics of High Polymer Solutions. *J. Chem. Phys.* **1942**, *10*, 51−61.

(63) Huggins, M. L. Solutions of Long Chain Compounds. *J. Chem. Phys.* **1941**, *9*, 440.

(64) Favre, E.; Nguyen, Q. T.; Clement, R.; Neel, J. Application of Flory-Huggins theory to ternary polymer-solvents equilibria: A case study. *Eur. Polym. J.* **1996**, *32*, 303−309.

(65) Diamond, A. D.; Hsu, J. T. Fundamental studies of biomolecule partitioning in aqueous two-phase systems. *Biotechnol. Bioeng.* **1989**, *34*, 1000−1014.

(66) Matsen, M. W.; Bates, F. S. Unifying weak- and strong-segregation block copolymer theories. *Macromolecules* **1996**, *29*, 1091−1098.

(67) Hietala, S.; Strandman, S.; Järvi, P.; Torkkeli, M.; Jankova, K.; Hvilsted, S.; Tenhu, H. Rheological properties of associative star polymers in aqueous solutions: Effect of hydrophobe length and polymer topology. *Macromolecules* **2009**, *42*, 1726−1732.

(68) Wang, S.; Larson, R. G. Multiple relaxation modes in suspensions of colloidal particles bridged by telechelic polymers. *J. Rheol.* **2018**, *62*, 477−490.

(69) Travitz, A.; Larson, R. G. Brownian Dynamics Simulations of Telechelic Polymers Transitioning between Hydrophobic Surfaces. *Macromolecules* **2021**, *54*, 8612−8621.

(70) Malo de Molina, P.; Appavou, M.-S.; Gradzielski, M. Oil-in-water microemulsion droplets of TDMAO/decane interconnected by the telechelic C18-EO150-C18: Clustering and network formation. *Soft Matter* **2014**, *10*, 5072−5084.

I

(71) Puech, N.; Mora, S.; Testard, V.; Porte, G.; Ligoure, C.; Grillo, I.; Phou, T.; Oberdisse, J. Structure and rheological properties of model microemulsion networks filled with nanoparticles. *Eur. Phys. J. E* **2008**, *26*, 13−24.

(72) Bae, Y. C.; Lambert, S. M.; Soane, D. S.; Prausnitz, J. M. Cloud-Point Curves of Polymer Solutions from Thermooptical Measurements. *Macromolecules* **1991**, *24*, 4403−4407.

(73) Krigbaum, W. R.; Geymer, D. O. Thermodynamics of Polymer Solutions. The Polystyrene-Cyclohexane System near the Flory Theta Temperature. *J. Am. Chem. Soc.* **1959**, *81*, 1859−1868.

(74) Smay, J. E.; Cesarano, J.; Lewis, J. A. Colloidal Inks for Directed Assembly of 3-D Periodic Structures. *Langmuir* **2002**, *18*, 5429−5437.
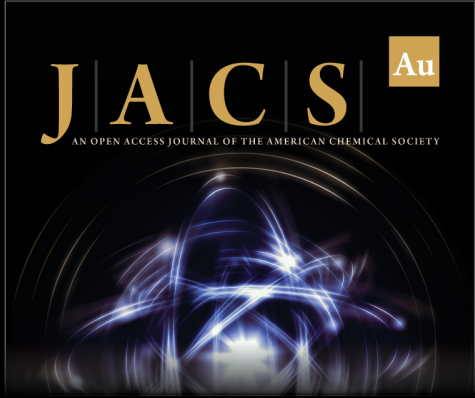
(75) Compton, B. G.; Lewis, J. A. 3D-printing of lightweight cellular composites. *Adv. Mater.* **2014**, *26*, 5930−5935.

(76) Daly, A. C.; Riley, L.; Segura, T.; Burdick, J. A. Hydrogel microparticles for biomedical applications. *Nat. Rev. Mater.* **2020**, *5*, 20−43.

(77) Chao, Y.; Chen, Q.; Liu, Z. Smart Injectable Hydrogels for Cancer Immunotherapy. *Adv. Funct. Mater.* **2020**, *30*, 1902785.

(78) Saha, K.; Keung, A. J.; Irwin, E. F.; Li, Y.; Little, L.; Schaffer, D. V.; Healy, K. E. Substrate modulus directs neural stem cell behavior. *Biophys. J.* **2008**, *95*, 4426−4438.

(79) Caliari, S. R.; Burdick, J. A. A practical guide to hydrogels for cell culture. *Nat. Methods* **2016**, *13*, 405−414.